# An Improved Nonlinear Cross-Coupled Control Strategy for Dual-Motor System Based on CM/DM Separation

Shuai Li, *Student Member, IEEE*, Xuewei Xiang, *Member, IEEE*, Hui Li, *Member, IEEE*, and Yunyan Wu

***Abstract*—In dual-motor system, uncertain disturbance, parameter differences, and mechanical issues deteriorate the synchronization. Moreover, motor collision problem arises in rigidly connected systems because of poor synchronization and transient large impact. Considering these factors, this article proposes a nonlinear cross-coupled control strategy based on common mode differential mode (CM/DM) separation to achieve position synchronization for dual-motor system under speed control. By utilizing the CM/DM separation method in cross-coupled control, the objectives of position synchronization control and speed tracking control is decoupled. Taking into account the collision model, mechanical clearance, disturbance, and real-time status of the dual-motor system, a nonlinear controller is designed to achieve high-accuracy synchronization and collision recovery. The stability of the dual-motor system is proved by analysis of frequency domain and nonlinear differential equations, and the tuning method for the proposed controller is provided. By comparison with the traditional cross-coupled control method, the effectiveness of the proposed control strategy is validated by experimental results.**

***Index Terms*—Cross-coupled control (CCC) strategy based on common mode differential mode (CM/DM) separation, collision recovery, CCC, dual-motor system, nonlinear control.**

## I. Introduction

With the development of modern industrial technology, equipment with only one motor can hardly satisfy the power requirement. Thus, dual-motor system has been widely used in various industrial applications, e.g., transmission, processing, and manufacturing [1], [2], [3]. Moreover, synchronous operation of two motors has extra advantages including higher volumetric efficiency, balanced distribution of power and long service life, etc.

Received 13 June 2024; revised 26 September 2024; accepted 31 October 2024. Date of publication 7 November 2024; date of current version 18 December 2024. This work was supported in part by the National Natural Science Foundation of China under Grant 52207037, in part by the National Key Research and Development Program of China under Grant 2022YFB4702100, and in part by the National Key Laboratory of Electromagnetic Energy under Grant 61422172220203. Recommended for publication by Associate Editor Lakshmi Varaha Iyer. *(Corresponding authors: Xuewei Xiang; Hui Li.)*

The authors are with the State Key Laboratory of Power Transmission Equipment Technology, School of Electrical Engineering, Chongqing University, Chongqing 400044, China (e-mail: ShuaiLi@stu.cqu.edu.cn; xueweixiang@cqu.edu.cn; cqulihui@cqu.edu.cn; wuyy@stu.cqu.edu.cn).

Color versions of one or more figures in this article are available at https://doi.org/10.1109/TPEL.2024.3493970.

Digital Object Identifier 10.1109/TPEL.2024.3493970

Gears and screws are two typical rotors in dual-motor systems, with additional types of rotors including circular arc rotors and involute rotors. Under the premise of no metal-to-metal contact of the twin rotors, the mechanical structures of these rotors enable the equipment to execute diverse functions including gas evacuation and discharge, liquid pumping and drainage, material transfer and mixing, as well as melting and homogenization process [4], [5].

The most straightforward approach to realize synchronous operation is to connect two motors via gears. They are referred to as timing gears and installed on the lateral sides of the rotors. Timing gears are typically lubricated with oil and their mechanical clearance is smaller than that of the twin rotors, thus serving the purpose of power transmission and protection of the rotor. However, there are problems such as low synchronization accuracy, wear, and even deformation of mechanical structure [6]. Connecting two motors in parallel for operation is also a viable approach [7], [8]. Although this method enjoys higher economic feasibility due to the need for only one inverter, it is not suitable for applications that demand high-accuracy synchronization. In order to ensure the normal operation of the equipment, it is supposed to control the position deviation within the mechanical clearance of the twin rotors. However, mechanical clearance of the twin rotors is generally quite small, significantly increasing the difficulty of achieving synchronization. Moreover, when the synchronization performance deteriorates or the system is subjected to instantaneous large impact, mechanical collision will occur, causing damage to the equipment. The accuracy of synchronous control still needs to be improved.

As a consequence, many synchronous control strategies have been proposed to obtain a satisfactory synchronization performance. General synchronous schemes for dual-motor system include master , electrical virtual line-shafting and cross-coupled. Master–slave scheme takes the output of the master motor as the given input for the slave motor [9], [10]. Due to the fact that the master motor is not influenced by the slave motor, the system exhibits poor antidisturbance ability. The electrical virtual line-shafting scheme has a better synchronization performance but there exists static error in speed tracking [11]. Cross-coupled control (CCC) scheme is first proposed in [12], it feeds back the speed deviation to the control quantity of each motor. In this way, the two motors can be adjusted simultaneously, achieving

better synchronization. Since then, the CCC method has received widespread attention. However, the closed-loop of speed of two motors will interact with the cross-coupled feedback, leading to contradiction of speed tracking and synchronization [13]. To address this issue, in [14], different bandwidths of speed regulator and synchronization error regulator are designed to decouple speed loop and cross-coupled loop. However, the separation boundary of bandwidth is blurry. In addition, efforts have been made to improve the structure of CCC. In [15], an additional coupling feedback loop with a second-order global fast terminal sliding mode controller is appended to CCC. In [16], considering the speed loops of two motors as a whole, a unified speed loop model is established. These methods are of interest to improve the anti-interference ability and dynamic performance, the contradiction is still failed to be resolved radically. In [17], a ring network control structure is established. Although the coupling in control is partly solved by combining advantages of CCC and master–slave control, dynamic performance is sacrificed to some extent.

In addition, the rapidity and accuracy of synchronization are highly sensitive to the feedback coefficient. Better transient response requires significant feedback coefficient, but increasing the coefficient will cause oscillations and even lead to instability [18]. In order to obtain better synchronization accuracy and dynamic performance, researchers have combined CCC with many advanced algorithms, including adaptive control [19], sliding-mode control [15], fuzzy logic [20], neural networks [21], and MPC [22]. However, these algorithms fail to take into account issues such as digital delay and mechanical collision. Moreover, the challenges in control parameters tuning, reliance on model accuracy and mitigation of computation burden are also limitations of these algorithms.

Given the issues mentioned above, a nonlinear CCC strategy for dual-motor system based on CM/DM separation is proposed to improve the position synchronization and address collision problem under speed closed-loop control. The main contributions of this article are as follows.

1) To address the problem that cross-coupled feedback interacts with the speed closed-loop, a CM/DM control structure is designed to decouple them. The disturbances are separated into CM and DM. They are regulated by CM loop and DM loop, respectively.
2) A nonlinear controller with a low computational amount is designed. The controller is mainly marked by a nonlinear function and a restitution coefficient. The former is to obtain a better dynamic performance and the latter is to facilitate collision recovery and accelerate convergence. Through frequency domain analysis and solving nonlinear differential equations, the stability of the system is proved.
3) Considering mechanical clearance and digital delays, the tuning method for the proposed controller is given. The designed system is proven to possess excellent antidisturbance performance.

The rest of this article is organized as follows. Section II consists the system description and preliminaries. Section III presents the establishment of the CM/DM-CCC. In Section VI, a nonlinear controller is proposed. In Section V, the analysis of stability and antidisturbance is presented. In Section VI, the effectiveness of the proposed control strategy is verified by experimental results. Finally, Section VII concludes this article.

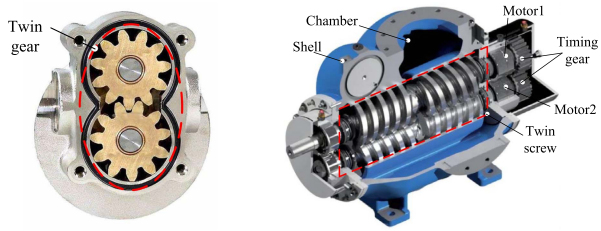


Fig. 1. Two typical rotors and their mechanical structures in dual-motor systems.

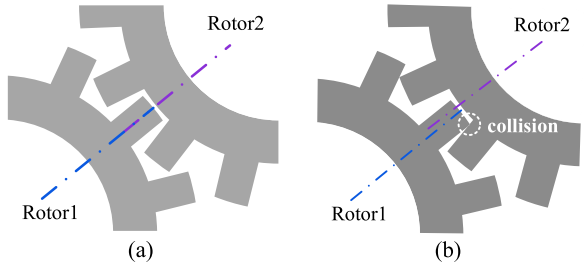


Fig. 2. Dual-motor's mechanical clearance. (a) In ideal condition. (b) In collision condition.

## II. System Description and Preliminaries

### A. Problem Formulation

Two typical twin rotors and their mechanical structures in dual-motor systems are shown as Fig. 1. Unlike the rotors in dual-motor servo systems or dual-motor driving systems, the primary function of the rotors is not for driving [23], [24]. In order to realize the function of the equipment, the twin rotors are supposed to operate at the same speed without metal-to-metal contact. Considering the mechanical clearance which can be illustrated as Fig. 2, the position deviation of the two motors is constrained within a small range, greatly improving the requirement of control accuracy. Moreover, mechanical collision problem occurs in such system and remains to be solved.

The simplified dynamics equations of dual-motor system can be written as

$$\begin{cases} \ddot{\theta}_x = \dot{\omega}_x = (K_{tx} i_x - T_{Lx})/J_x \\ \delta = \theta_1 - \theta_2 < \theta_{\max} \end{cases} \tag{1}$$

where $x = 1, 2$, representing different motor. $\theta_x$, $\omega_x$, $K_{tx}$, $i_x$, $J_x$, $T_{Lx}$, $\theta_{\max}$, and $\delta$ are the angular position, angular velocity, torque coefficient, current, inertia, load disturbance, mechanical clearance, and position deviation, respectively.

The traditional CCC (TCCC) strategy for dual-motor system is described as Fig. 3, two motors need to run synchronously at set speed $\omega^*$. There exists a coupling between the coupling controller and two speed controllers, the corresponding torque produced by them may be contradictory. Such contradiction of

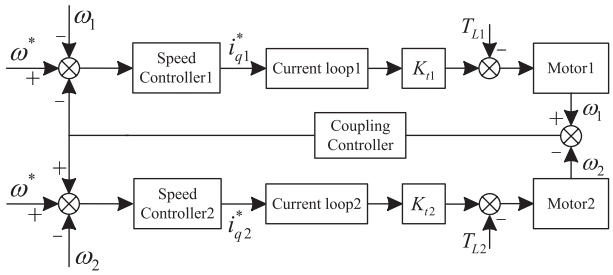


Fig. 3. Block diagram of TCCC strategy.

control finally results in oscillation and even cause collisions. The coupling controller is usually designed as a proportional or PI. Since the disturbances of the dual-motor system are influenced by multiple factors [25], these two type controllers can hardly achieve ideal synchronization performance in both dynamic and steady-state aspect. It is difficult to set the parameters to ideal in practice.

### B. Overall Synchronization Control Strategy

The proposed control strategy in this article and the whole system are shown as Fig. 4. Both motors are controlled through $i_d = 0$ strategy. The two motors are equipped with twin screw and supposed to achieve position synchronization under $\omega^*$. To improve the synchronization accuracy and achieve collision recovery, the controlled quantities ($\omega$, $\theta$, $i_q$, and torque) are separated into CM and DM and considered, respectively. Taking into account factors such as mechanical differences and demagnetization, motors' parameters ($J$ and $K_t$) are also separated into CM and DM. CM/DM-CCC is established to realize CM/DM separation. Nonlinear coupling controller regulates the DM component and output the DM current reference $i^*_{\mathrm{DM}}$ back. Detailed analysis will be given in the following sections.

## III. Proposed CM/DM-CCC Method

The block diagram of the proposed method is shown as Fig. 5. In servo applications, the most inner control loop has the fastest response speed. So based on TCCC method, the output of the coupling controller is directly compensated to the current reference [26]. The input of the coupling controller is the difference of two motors' positions. The two motors share one speed loop together and the feedback speed is the weighted average of their speeds based on their $J$. Improved differentiation algorithm is adopted in the calculation of $\omega_f$ to minimize error [27]. The outputs of the speed controller and coupling controller are presented as $i^*_{\mathrm{CM}}$ and $i^*_{\mathrm{DM}}$*, respectively, which are proportionally distributed according to the two motors' $K_t$.

It should be noted that the outputs of both the unified speed controller and the coupling controller are torque references. Since $i_d = 0$ strategy is adopted in this article, the torque reference is equivalent to $i^*_q$. If other control strategies are used, such as MTPA and field-weakening control, it is necessary to additionally convert the torque reference into current reference.

In the signal analysis, signals are often separated into CM and DM. Similarly, the disturbance of the two motors $T_{L1}$ and $T_{L2}$ can also be separated into CM disturbance $T_{Lc}$ and DM disturbance $T_{Ld}$, which is shown as

$$\begin{aligned} T_{L1} &= \frac{T_{L1}+T_{L2}}{2} + \frac{T_{L1}-T_{L2}}{2} = T_{Lc} + T_{Ld} \\ T_{L2} &= \frac{T_{L1}+T_{\mathrm{L2}}}{2} - \frac{T_{L1}-T_{L2}}{2} = T_{Lc} - T_{Ld}. \end{aligned} \tag{2}$$

$T_{Lc}$ and $T_{Ld}$ produce perturbations in the speed and position. For the TCCC method, coupling controller and speed controllers will regulate these perturbations simultaneously, leading to mutual influence in control.

For the CM/DM-CCC method in Fig. 5, the electromagnetic torque of the two motors can be obtained as

$$\begin{aligned} T_{e1} &= K_{t1}L_{c1}i^*_{\mathrm{CM}} + K_{t1}L_{c1}i^*_{\mathrm{DM}} \\ T_{e2} &= K_{t1}L_{c2}i^*_{\mathrm{CM}} - K_{t1}L_{c2}i^*_{\mathrm{DM}} \end{aligned} \tag{3}$$

where $L_{cx}$ represents the transfer function of the current loop that includes the motor itself, current controller, filter, and inverter. By designing the current controllers of two motors, we can assume that $L_{c1} = L_{c2} = L_c$. Therefore, (3) can be written as

$$T_{e1} = T_{ec} + T_{ed} \qquad T_{e2} = T_{ec} - T_{ed} \tag{4}$$

with

$$\begin{aligned} T_{ec} &= K_{t1}L_c i^*_{\mathrm{CM}} \\ T_{ed} &= K_{t1}L_c i^*_{\mathrm{DM}}. \end{aligned} \tag{5}$$

The electromagnetic torque of the two motors is separated into CM and DM. $T_{ec}$ and $T_{ed}$ correspond to the outputs of unified speed controller and coupling controller, respectively.

By substituting (2) and (4) into (1), and based on Fig. 5, the speed feedback $\omega_f$ can be obtained as

$$\begin{aligned} \omega_f &= s\frac{J_1\left(\frac{T_{e1}-T_{L1}}{s^2J_1}\right) + J_2\left(\frac{T_{e2}-T_{L1}}{s^2J_2}\right)}{J_1+J_2} \\ &= \frac{T_{ec}-T_{Lc}}{s\left(J_1+J_2\right)} \end{aligned} \tag{6}$$

which only engages the CM disturbance. We can also get the input of coupling controller $\delta$ as

$$\begin{aligned} \delta = \frac{T_{e1}-T_{L1}}{s^2J_1} - \frac{T_{e2}-T_{L2}}{s^2J_2} = \left(\frac{1}{J_1}+\frac{1}{J_2}\right) \\ \frac{\left(T_{ed}-T_{Ld}\right)}{s^2} + \left(\frac{1}{J_1}-\frac{1}{J_2}\right)\frac{\left(T_{ec}-T_{Lc}\right)}{s^2}. \end{aligned} \tag{7}$$

For dual-motor systems that satisfy $J_1 = J_2$, (7) can be simplified as

$$\delta = \left(\frac{1}{J_1}-\frac{1}{J_2}\right)\frac{T_{ed}-T_{Ld}}{s^2} \tag{8}$$

which implies that only DM disturbance affects synchronization. For dual-motor systems that satisfy $J_1 \neq J_2$, due to the different acceleration of two motors after being disturbed, coupling controller needs to adjust this factor extra.

According to (5)–(7), the unified speed controller and the coupling controller are utilized for CM regulation and DM

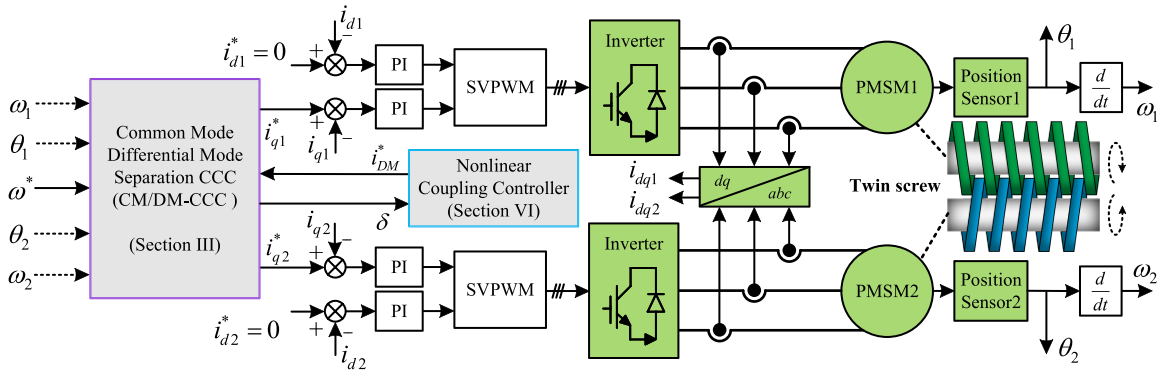


Fig. 4. Block diagram of the overall synchronization control strategy.

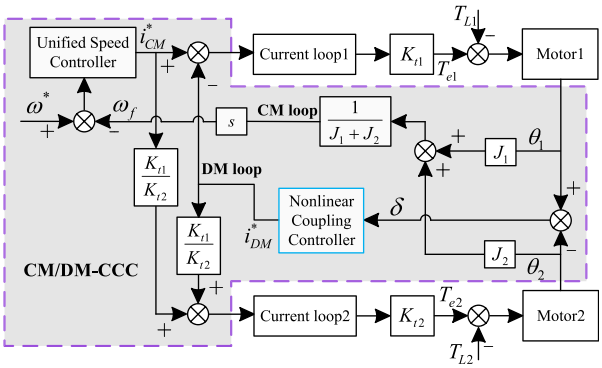


Fig. 5. Block diagram of CM/DM-CCC strategy.

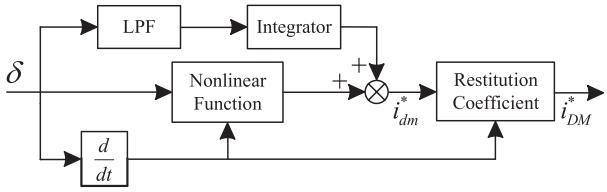


Fig. 6. Block diagram of nonlinear controller.

regulation, respectively. It can be checked that the adjustment of coupling controller will not affect the weighted average speed, namely, not interact with the unified speed controller.

The position deviation $\delta$ contains factors that affect synchronization in the dual-motor system, including disturbance and parameter differences. We define these factors as DM factors. Hence, the whole control structure in Fig. 5 is separated into CM loop and DM loop. The weighted average speed is independent of DM factors. Similarly, the synchronization performance will maintain ideal when changes happen in CM loop, even if there is oscillation or overshoot in unified speed controller. The synchronization performance can be improved by designing the coupling controller,

## IV. Nonlinear Coupling Controller

Based on CM/DM separation in Section III, we can only focus on DM factors in the following analysis. According to Newton's Third Law, the collision between two motors can be analyzed as a DM disturbance, and it consequently will be discussed in this section.

### A. Structure of Nonlinear Coupling Controller

Assume parameter differences as the result of disturbances and $\delta$ is affected by an equivalent DM disturbance $T_{Ld}^*$, which is unknown. Equation (7) can be replaced as

$$\delta = \left(\frac{1}{J_1} + \frac{1}{J_2}\right)\frac{T_{ed} - T_{Ld}^*}{s^2}. \tag{9}$$

The Fourier decomposition of $T_{Ld}^*$ can be derived as

$$T_{Ld}^* = A_0 + \sum_{k=1}^{\infty} A_k e^{j\omega k t}. \tag{10}$$

The structure of proposed nonlinear controller is shown as Fig. 6. The integrator is able to regulate the dc component in $T_{Ld}^*$. The low-pass filter makes it works at low frequency only, avoiding affecting the adjustment of the nonlinear part. Nonlinear function is developed to limit ac component and achieve fast response. The restitution coefficient is designed to achieve collision recovery and convergence of $\delta$.

### B. Nonlinear Function

Considering the role of LPF, the integrator can be neglected during the nonlinear part analysis. Using motor1 as the reference frame ($\theta_1 = 0$), the range of $\delta$ is $(-\theta_{\max}, +\theta_{\max})$. The torque that $i_{\mathrm{dm}}^*$ produces is represented as $T_{\mathrm{dm}}^*$ ($T_{\mathrm{DM}}^*$ corresponds to $i_{\mathrm{DM}}^*$), which can be obtained by

$$T_{\mathrm{dm}}^* = \frac{3}{2} p_n i_{\mathrm{dm}}^* \psi_f \tag{11}$$

where $p_n$ is the pole pairs, $\psi_f$ is the flux linkage from the permanent magnet. The condition for not producing collisions

at any $\delta$ can be expressed as

$$\begin{cases} \theta_1+\theta_2=\theta_{\max}-\delta & \left(\dot{\delta}>0\right) \\ \theta_1+\theta_2=\theta_{\max}+\delta & \left(\dot{\delta}<0\right) \\ \frac{3}{2}p_n\psi_f k\left(\int_0^{\theta_1}\delta d\delta+\frac{J_2}{J_1}\int_0^{\theta_2}\delta d\delta\right)\geq\frac{1}{2}J_2\dot{\delta}^2 \end{cases} \tag{12}$$

where $k$ is gain of the nonlinear function. It can be derived that

$$k_{\min}\leq k_1=\begin{cases} \frac{8\sqrt{2}\dot{\delta}^2\max(J_1,J_2)}{3p_n\psi_f(\theta_{\max}-\delta)^3} & \left(\dot{\delta}>0\right) \\ \frac{8\sqrt{2}\dot{\delta}^2\max(J_1,J_2)}{3p_n\psi_f(\theta_{\max}+\delta)^3} & \left(\dot{\delta}<0\right) \end{cases} \tag{13}$$

where $k_{\min}$ is the minimum $k$ in (12). $k_1$ is a variable parameter based on mechanical clearance, $\delta$ and $\dot{\delta}$. Such method avoids fussy parameter calibration. In addition, collision can be avoided as long as the current reference is within the bandwidth of current loop. However, the dual-motor system may operate in a state of high proximity to collision, resulting in unsatisfactory synchronization accuracy.

In order to solve this problem and improve transient response, we set a $k_2$ which can be expressed as

$$k_2=\frac{\alpha}{|\delta|}. \tag{14}$$

According to Fig. 6, $i^*_{\rm dm}$ is a sign function of $\delta$ under $k_2$, which ensures that the controller can achieve a significant gain when $\delta$ is small. Later in this article, we will analyze that $k_2$ can also improve disturbance rejection ability. In order to simultaneously obtain the effects of $k_1$ and $k_2$, as a result, the nonlinear function is designed as

$$k=\max(k_1,k_2). \tag{15}$$

In Section V, the stability and performance of the system are verified and the tuning method of $\alpha$ will be provided.

### C. Restitution Coefficient

When dual-motor system is encountered to a transient large impact and the current loop is unable to adjust in time, the two motors will be forced to operate synchronously via timing gears, however, resulting in collisions. The restitution coefficient $r$ is implemented as

$$r=\begin{cases} 1 & \dot{\delta}\delta>0 \\ e^{-\beta\dot{\delta}} & \dot{\delta}\delta<0. \end{cases} \tag{16}$$

Assume $k$ is constant and use motor1 as the reference frame, with restitution coefficient adopted, the dual-motor's operation state can be illustrated as Fig. 7.

The value of $\delta$ and $\dot{\delta}$ at $t_i$ can be represented as $\delta(i)$ and $\dot{\delta}(i)$. In Fig. 7, the two motors cross the mid line with a relative speed $\dot{\delta}(0)$, then they collide at $t_1$. According to momentum conservation, $\dot{\delta}$ before and after the first collision are $+\dot{\delta}(1)$ and $-\dot{\delta}(1)$. The two motors return to mid line with a relative speed $\dot{\delta}(2)$. After $t_{2n}$, the collisions end. The work done by $T^*_{\rm DM}$ before and after the collision is define as $Q_l$ and $Q_b$, the work done by the $T^*_{Ld}$ is $Q_D$. Given that the value of $k_1$ is significant during

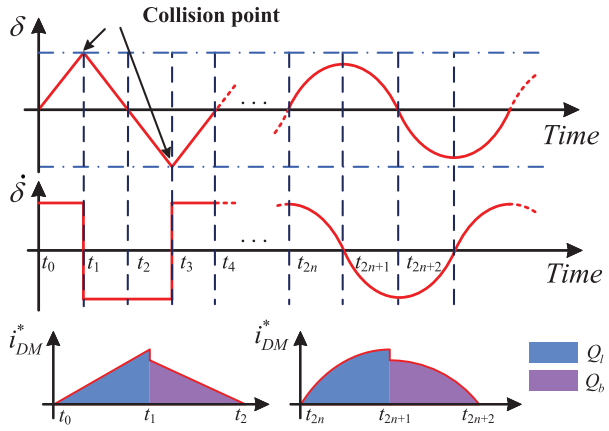


Fig. 7. $\delta$ and $\dot{\delta}$ of the two motors and the corresponding $i^*_{\rm DM}$ under restitution coefficient.

the collision process, (15) can therefore be written as $k=k_1$. The following assumption is made.

*Assumption 1:* During the collisions, $Q_l$ and $Q_b$ are large enough so that we can assume $Q_l\gg Q_D$ and $Q_b\gg Q_D$.

It can be obtained that

$$\begin{cases} \frac{1}{2}J_2\dot{\delta}^2(0)-\frac{1}{2}J_2\dot{\delta}^2(1)=Q_{\rm l} \\ \frac{1}{2}J_2\dot{\delta}^2(2)-\frac{1}{2}J_2\dot{\delta}^2(1)=Q_{\rm b} \end{cases} \tag{17}$$

which can be simplified as

$$\frac{1}{2}J_2\dot{\delta}^2(0)-\frac{1}{2}J_2\dot{\delta}^2(2)=Q_{\rm l}-Q_{\rm b}=\Delta Q. \tag{18}$$

The value of $Q_l$ and $Q_b$ determines the value of $\dot{\delta}$ during collisions. Due to the restitution coefficient, $Q_l$ and $Q_b$ obviously satisfy $Q_l>Q_b$. Thus, we can get that $|\dot{\delta}(0)|>|\dot{\delta}(2)|$. Then, collision will occur again at $t_3$. Through iteration of (18), we can obtain

$$|\dot{\delta}(0)|>|\dot{\delta}(2)|>|\dot{\delta}(4)|>\cdots>|\dot{\delta}(2n)|. \tag{19}$$

Finally, $\dot{\delta}$ reaches the critical value $\dot{\delta}(2n)$ and collision ends. The value of $\Delta Q$ determines the convergence speed of $\dot{\delta}$ and is positively correlated with it. It is worth noting that such method can help $\delta$ converge when no collision happens (after $t_{2n}$). But in this case, the work done by disturbance cannot be neglected, i.e., *Assumption 1* is invalid. An excessively large value of $\Delta Q$ may result in $\delta$ being unable to return to zero. According to (16), $r$ increases with $\dot{\delta}$ decreasing, ensuring $Q_b>Q_D$ so that $\delta$ is able to return back to zero when $\delta\dot{\delta}<0$.

A smaller $r$ is obtained when $\dot{\delta}$ is large, causing $\delta$ to converge at a fast rate. $r$ will be closed to one after $\dot{\delta}$ tends to stabilize or gets small, which makes certain that $|T^*_{\rm DM}|>|T^*_{Ld}|$. The restitution coefficient guarantees the coverage of $\delta$ and system's stability.

## V. Stability and Antidisturbance Analysis

### A. Stability Analysis

With the effect of time-varying parameter $k_1$ and restitution coefficient $r$, $k_1$ will gradually decrease to a value less than $k_2$.

The nonlinear function can always reach

$$k = \max(k_1, k_2) = k_2. \tag{20}$$

Since $\dot{\delta}$ in (16) is relatively small at this time, $r$ is temporarily neglected and $i^*_{\mathrm{DM}}$ can be derived as

$$i^*_{\mathrm{DM}} = k \times \delta = \alpha \operatorname{sgn} \delta. \tag{21}$$

According to (10), providing that there is an unknown ac component $T_k$ with an amplitude of $A_k$ and a frequency of $f_k$. $T_k$ can be expressed as

$$T_k = A_k \cos \omega_k t. \tag{22}$$

Through analysis of momentum and impulse we can get

$$J_x \omega = \frac{A_k}{\omega_k} \sin \omega_k t - T^*_{\mathrm{DM}} \int_0^t \operatorname{sgn} \delta d\tau. \tag{23}$$

The integral of (23) can be derived as

$$\delta = \frac{A_k}{\omega_k J_x} \left(1 - \frac{1}{\omega_k} \cos \omega_k t\right) - \frac{T^*_{\mathrm{DM}}}{J_x} \int_0^t d\tau \int_0^t \operatorname{sgn} \delta d\tau. \tag{24}$$

The second-order derivative of (24) is given by

$$\ddot{\delta}(t) = \frac{A_k}{J_i} \cos \omega_k t - \frac{T^*_{\mathrm{DM}}}{J_i} \operatorname{sgn} \delta(t). \tag{25}$$

The encoders of the two motors feedback position signals simultaneously, and $\delta$ is processed within the same control interval. Consequently, there is no delay between $\theta_1$ and $\theta_2$. However, the delay caused by computation delay and sampling update in the digital controller exists and is supposed to be considered. We add a delay to (25) as

$$\ddot{\delta}(t+d) = \frac{A_k}{J_i} \cos \omega_k t - \frac{T^*_{\mathrm{DM}}}{J_i} \operatorname{sgn} \delta(t) \tag{26}$$

where $d$ represents the delay time. As an approximation to the solution, we use the truncated Fourier series

$$\delta(t+d) = a' \cos(\omega(t+d)) + b' \sin(\omega(t+d)) \tag{27}$$

which can be rewrite as

$$\delta(t+d) = a \cos \omega t + b \sin \omega t \tag{28}$$

with

$$\begin{aligned} a &= a' \cos \omega d + b' \cos \omega d \\ b &= -a' \sin \omega d + b' \cos \omega d. \end{aligned} \tag{29}$$

Disregarding of higher harmonics [28], $\operatorname{sgn} \delta$ can be expressed as

$$\begin{aligned} \operatorname{sgn}\{\delta(t)\} = &\frac{4a}{\pi\sqrt{(a^2+b^2)}} \cos \omega_k t \\ &+ \frac{4b}{\pi\sqrt{(a^2+b^2)}} \sin \omega_k t + \text{higherharmonics}. \end{aligned} \tag{30}$$

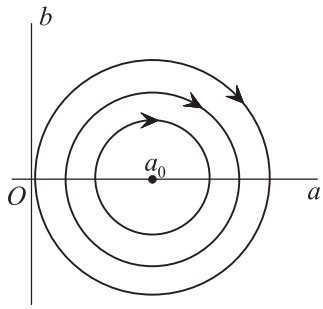


Fig. 8. Path near $(a_0, 0)$ in the van der Pol phase plane.

Substituting (28) and (30) into (25), it can be derived that

$$\begin{cases} \frac{A_k}{J_x} + a\omega_k^2 - \frac{4aT^*_{\mathrm{DM}}}{J_x \pi \sqrt{(a^2+b^2)}} = 0 \\ b\omega_k^2 - \frac{4bT^*_{\mathrm{DM}}}{J_x \pi \sqrt{(a^2+b^2)}} = 0. \end{cases} \tag{31}$$

The solution of (31) can be expressed as

$$\begin{cases} a\left(4T^*_{\mathrm{DM}} - \pi |a| \omega_k^2 J_i\right) = A_k \pi |a| \\ b = 0. \end{cases} \tag{32}$$

To investigate stability, transient state analysis is necessary. By supposing the coefficients $a$ and $b$ are slowly varying functions of time, it can be determined that whether the transient state of $\delta$ lead to or away from periodic states. Assume that

$$\delta(t) = a(t) \sin \omega_k t + b(t) \cos \omega_k t \tag{33}$$

where $a$ and $b$ are slowly varying amplitudes (compared with $\cos(\omega_k t)$ and $\sin(\omega_k t)$). Ignoring $\ddot{a}$ and $\ddot{b}$ we can get

$$\begin{aligned} \ddot{\delta}(t) \approx &\left(-\omega_k^2 a + 2\omega_k \dot{b}\right) \cos \omega t \\ &+ \left(-2\omega_k \dot{a} - \omega_k^2 b^2\right) \sin \omega_k t. \end{aligned} \tag{34}$$

Combining (25), (30), (33), and (34), there is

$$\begin{cases} \dot{a} = \frac{1}{2\omega_k} \left(-\omega_k^2 b + \frac{4bT^*_{\mathrm{DM}}}{J_x \pi \sqrt{(a^2+b^2)}}\right) \equiv A \\ \dot{b} = \frac{1}{2\omega_k} \left(\omega_k^2 a + \frac{A_k}{J_x} - \frac{4aT^*_{\mathrm{DM}}}{J_x \pi \sqrt{(a^2+b^2)}}\right) \equiv B. \end{cases} \tag{35}$$

Define $A_1(a,b) = \partial A_1(a,b)/\partial a$, $a_0$ is the solution of (32). We can derive

$$A_1(a_0, 0) = B_2(a_0, 0) = 0 \tag{36}$$

and

$$\begin{cases} A_2 = -\frac{\omega_k}{2} + \frac{4T^*_{\mathrm{DM}}}{|a_0|^3 \pi J_i} \\ B_1 = \frac{\omega_k}{2} - \frac{4T^*_{\mathrm{DM}}}{|a_0|^3 \pi J_i}. \end{cases} \tag{37}$$

The phase plane for $a$ and $b$ in the system is called the van der Pol plane, which is shown as Fig. 8. $(a_0, 0)$ is the equilibrium point of the system when $a_0 \neq 0$ is satisfied.

Substituting $a_0 \neq 0$ into (32), here is the stability condition

$$|T^*_{\mathrm{DM}}| > \frac{\pi}{4} A_k. \tag{38}$$

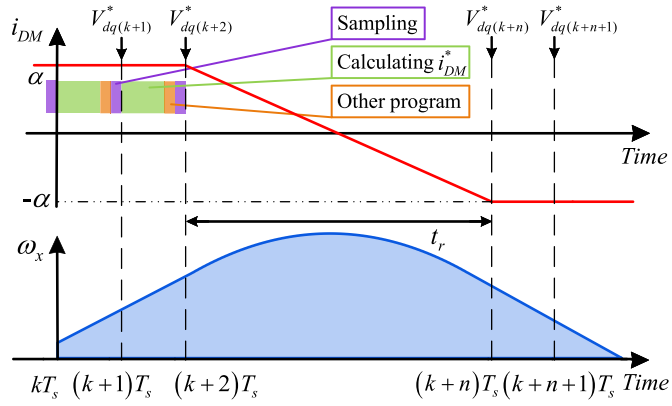


Fig. 9. Timing diagram of $i_{\mathrm{DM}}$ and $\omega_x$.

Considering the real-time control constraints and bandwidth of current loop, $\alpha$ is supposed to satisfy additional conditions.

As shown in Fig. 9. $T_s$ represents the sampling period. $i_{\mathrm{DM}}$ is the feedback DM current. One control interval can be divided into three parts, including sampling, calculation, and other program [29]. Motor crosses the mid line at $kT_s$ with an angular speed $\omega_x(kT_s)$ and a DM current where $i_{\mathrm{DM}} = i^*_{\mathrm{DM}} = \alpha$. Due to the control delay, $i^*_{\mathrm{DM}}$ becomes $-\alpha$ at $(k+2)T_s$. The time taken for $i_{\mathrm{DM}}$ to change from $\alpha$ to $-\alpha$ can be approximately represented as $t_r$, which is known as it is related to the bandwidth of current loop. After several intervals, $\omega_x$ reduces to zero and motor starts to return back. To avoid collision, the area of the blue part is limited by $\theta_{\max}$, which can be expressed as

$$\omega_{x0}\left(4T_s + t_r\right) + \frac{\alpha K_{t1}}{J_x}\left(2T_s + \frac{t_r^2}{12} + 2T_s t_r + 2T_s^2\right) + \frac{\omega_{x0} J_x}{2\alpha K_{t1}} < \theta_{\max} \tag{39}$$

where $\omega_{x0}$ equals $\omega_x(kT_s)$. By solving (39) we can obtain

$$\alpha < \frac{6J_x\theta_{\max} - 24J_x T_s\omega_{x0} - 6Jt_r\omega_{x0} + \sigma_1}{\sigma_2} \tag{40}$$

with

$$\begin{aligned}\sigma_1 &= \sqrt{6}J_x\sqrt{6\theta_{\max}^2 - 48\theta_{\max}T_s\omega_{x0} - 12\theta_{\max}t_r\omega_{x0}}\ldots \\ &\quad \sqrt{+96T_s^2\omega_{x0}^2 - 24T_s^2\omega_{x0} + 48T_s t_r\omega_{x0}^2}\ldots \\ &\quad \sqrt{-24T_s t_r\omega_{x0} - 24T_s\omega_{x0} + 6t_r^2\omega_{x0}^2} \\ \sigma_2 &= 24K_{t1}T_s^2 + 24K_{t1}T_s t_r + K_{t1}t_r^2.\end{aligned} \tag{41}$$

Due to the constraint of mechanical clearance and the effect of restitution coefficient, the value of $\omega_{x0}$ is generally within 0.5 rad/s. As a result, $\delta$ will be convergent when (38) and (40) are satisfied.

### B. Anti-Disturbance Analysis

Equation (38) suggests that the stability of the system is unrelated to $\omega_k$, $d$ and the direction of $T^*_{\mathrm{DM}}$.

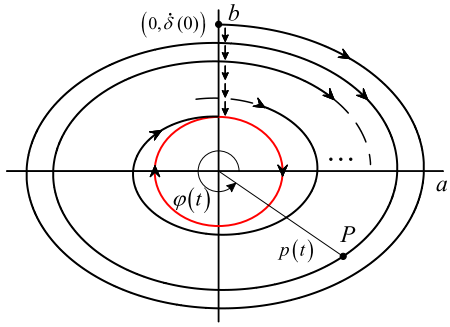


Fig. 10. Path in the van der Pol phase plane under restitution coefficient.

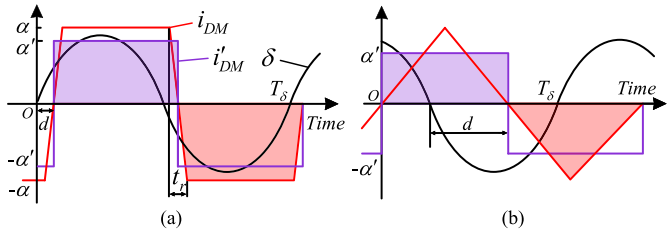


Fig. 11. $i_{\mathrm{DM}}$ and $\delta$ during the convergence process of $P$ toward the origin.

Among all the harmonics in (10), we define

$$A_{\max} = \max\left\{A_1, A_2, \ldots, A_k, \ldots, A_n\right\}. \tag{42}$$

Selecting an $\alpha$ which satisfies (40) and (43), the stability condition is reached for harmonics of all frequencies, demonstrating that the coupling controller is able to restrain the disturbance at all frequency

$$\left|\frac{3}{2}p_n\alpha\psi_f\right| > \frac{\pi}{4}A_{\max}. \tag{43}$$

If the path is closed in the van der Pol phase plane, (28) can be written as

$$\delta(t) = p(t)\cos\left(\omega t - \varphi(t)\right). \tag{44}$$

Assuming that $\dot{a}(0)$ is small, initial conditions can be obtained through (33), i.e.,

$$a(0) = \delta(0) \qquad b(0) = \dot{\delta}(0). \tag{45}$$

Combining the van der Pol phase plane with Fig. 7, the path under restitution coefficient can be shown as Fig. 10.

$P$ is a representative point on the closed path and it starts at $(0, \dot{\delta}(0))$. According to (18), $\dot{\delta}$ exhibits a continuous decrease, demonstrating that $p(t)$ keeps decreasing. The oscillation frequency of $\delta$ will increase as $P$ converges toward the origin. $P$ ultimately settles on the red path.

During the process of $P$ approaching the small neighborhood of the origin, $\delta$ and the corresponding $i_{DM}$ can be illustrated as Fig. 11.

$T_\delta$ is the oscillation period of $\delta$, and $i'_{\mathrm{DM}}$ represents the equivalent current, which can be expressed as $\alpha'\,\mathrm{sgn}\,\delta$. Obviously, $\alpha'$ is smaller than $\alpha$ due to $t_r$. $T_\delta$ decreases as $P$ approaches the red path, ultimately becoming less than $2t_r$. The condition for

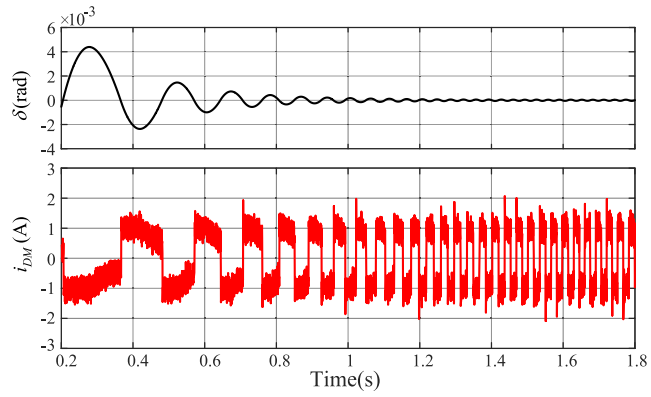


Fig. 12. Convergence of $\delta$ under disturbances and the corresponding $i_{\mathrm{DM}}$.

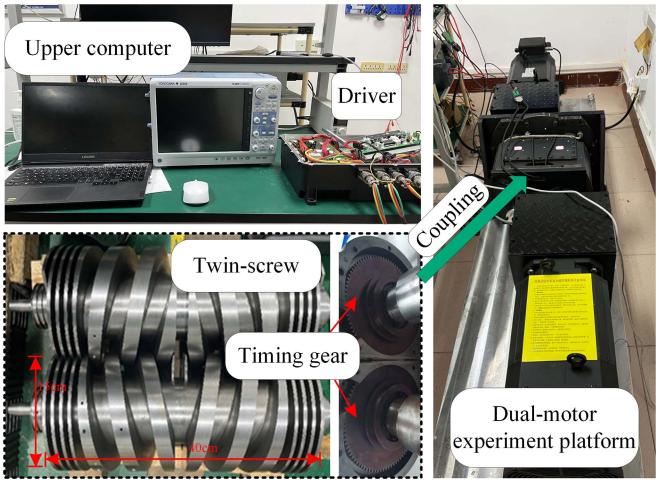


Fig. 13. Experiment system.

$i_{\mathrm{DM}}$ and $i'_{\mathrm{DM}}$ to be equivalent is that the areas of the red and purple parts are equal. We can replace $\alpha$ in (43) with $\alpha'$. As $\alpha'$ decreases to the critical value, $p(t)$ tends to stabilize, i.e., $\delta$ is a periodic function with a minimal amplitude under disturbance at any frequency. The simulation results shown in Fig. 12 validate the analysis above.

## VI. Experiment Results

To verify the effect of CM/DM nonlinear control (CDNC), Comparative experiments are carried out on the dual-motor system shown as Fig. 13.

Even with the implementation of synchronization control strategies, the installation of timing gears remains essential. The timing gears shown in Fig. 13 can protect the twin screw and enable forced synchronous operation in emergency situations. They feature a mechanical clearance of 0.01 rad ($\theta_{\max} = 0.01$ rad), which is smaller than that of the twin screw. Therefore, the experimental objective is to control the absolute value of $\delta$ to be at least within 0.01 rad or less, and to restore stable operation after collisions occur. The properties of two motors are given in Table I. The rated speed of motors is 4000 r/min and $p_n = 2$. The CDNC method proposed in Sections III and VI is implemented

TABLE I
Machine Properties

| Quantity | Value | Quantity | Value |
|---|---|---|---|
| $R_1$ | 0.4 Ω | $R_2$ | 0.38 Ω |
| $L_1$ | 4.5 mH | $L_2$ | 4.4 mH |
| $J_1$ | 0.004 kg.m$^2$ | $J_2$ | 0.004 kg.m$^2$ |
| $K_{t1}$ | 0.18 Nm/A | $K_{t2}$ | 0.18 Nm/A |

TABLE II
Different Situations

| Running situations | Working condition |
|---|---|
| Situation 1 | Speed up from 0 to 4000 r/min |
| Situation 2 | Steady at 4000 r/min |
| Situation 3 | Add unbalanced load at 4000 r/min |
| Situation 4 | Collision at 4000 and 500 r/min |

on the digital signal processor TMS28377D produced by Texas Instruments. CPU1 is used to control the two motors, CPU2 is used to transmit information and commands between the upper computer and motors. In CPU1, we set 3 control modes: CDNC mode, TCCC mode and no synchronization (NS) mode ($i^*_{\mathrm{DM}}$ in Fig. 6 is zero). Control mode can be switched via sending commands through the upper computer. The time-varying parameter $k_1$ in nonlinear function effectively avoids collision under normal operating conditions, even without the integrator. However, the removal of the integrator will cause the steady-state value of $\delta$ to deviate from zero. Hence, the primary objectives of designing LPF and integrator are to offset the dc component and mitigate the impact on nonlinear regulation, with the dynamic response being appropriately sacrificed. The value of $\beta$ is positively correlated with the convergence speed of $\delta$, and it has a broad range of values. However, an excessively large value of $\beta$ will deteriorate the steady-state performance. The setting range of $\alpha$ is given in Section V [formulas (38) and (40)]. The cutoff frequency of the LPF can be adjusted to a lower level, while the integral coefficient can be set to a higher value. The parameters of the proposed CDNC method are shown in (46). The LPF is designed as a second-order filter with a cutoff frequency of 5 Hz. Besides, the proportional and integral coefficients of the TCCC are $k_{p2} = 250$ and $k_{i2} = 50$. The control parameters of speed controllers and current controllers of two motors of two methods are identical and set up as well

$$\begin{cases} \alpha = 1 \\ \beta = 1 \\ k_{i1} = 500. \end{cases} \tag{46}$$

The experiment is divided into 4 situations, which is shown as Table II. Start the dual-motor system in CDNC mode and TCCC mode, respectively. Fig. 14(a) shows $\delta$ of the two control methods in situation 1. Through CDNC, $\delta$ is constrained within $\pm 0.003$ rad (1/3 of $\theta_{\max}$). There exists overshoot in the unified speed loop, but the synchronization performance is not affected. However, the TCCC has a poor synchronization performance and is prone to produce collisions.

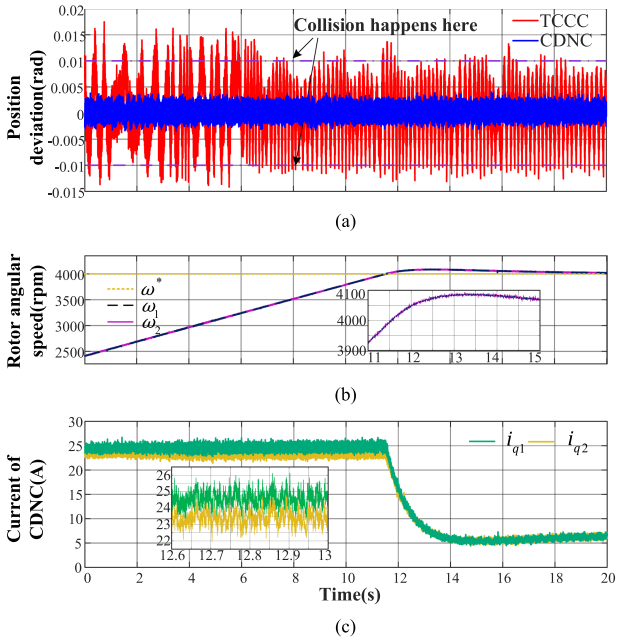


Fig. 14. Control performances in situation 1. (a) $\delta$ of the two control methods. (b) Two motors' speeds of CDNC. (c) Two motors' $i_q$ of CDNC.

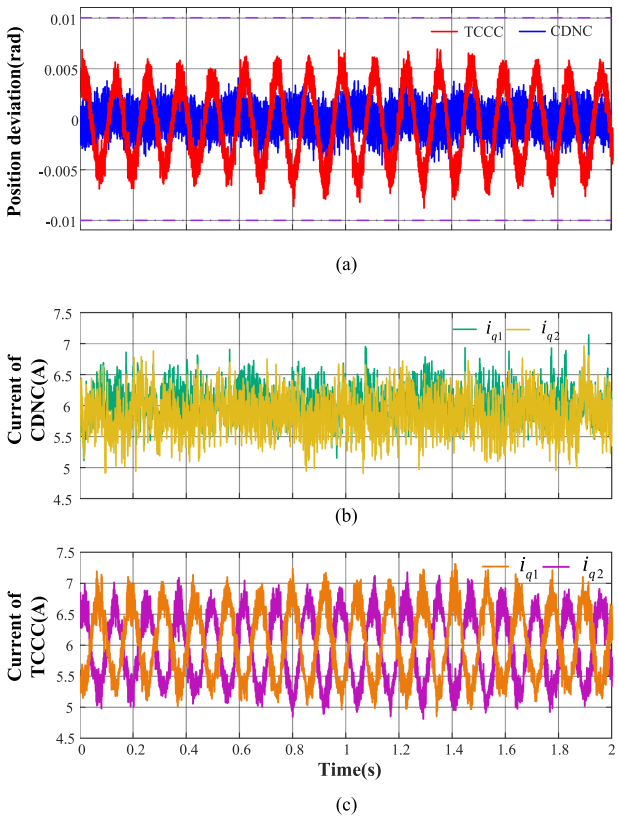


Fig. 15. Control performances in situation 2. (a) $\delta$ of the two control methods. (b) Two motors' $i_q$ of CDNC. (c) Two motors' $i_q$ of TCCC.

We start the motors in CDNC mode and switch to TCCC mode after reaching rated speed. Only in this way can TCCC obtain a stable operation. Fig. 15 shows $\delta$ and current of the two control methods in situation 2.

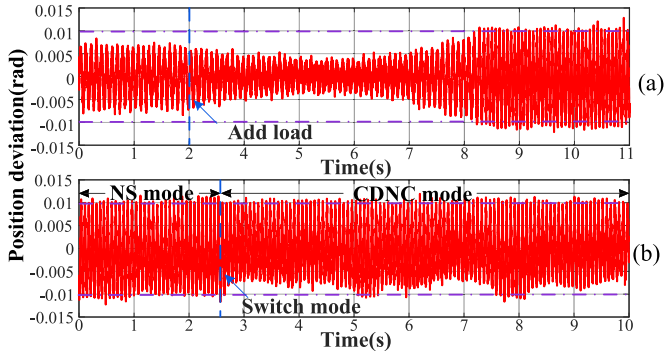


Fig. 16. Control performances of TCCC. (a) Add balanced load at 500 r/min. (b) Collision at 500 r/min.

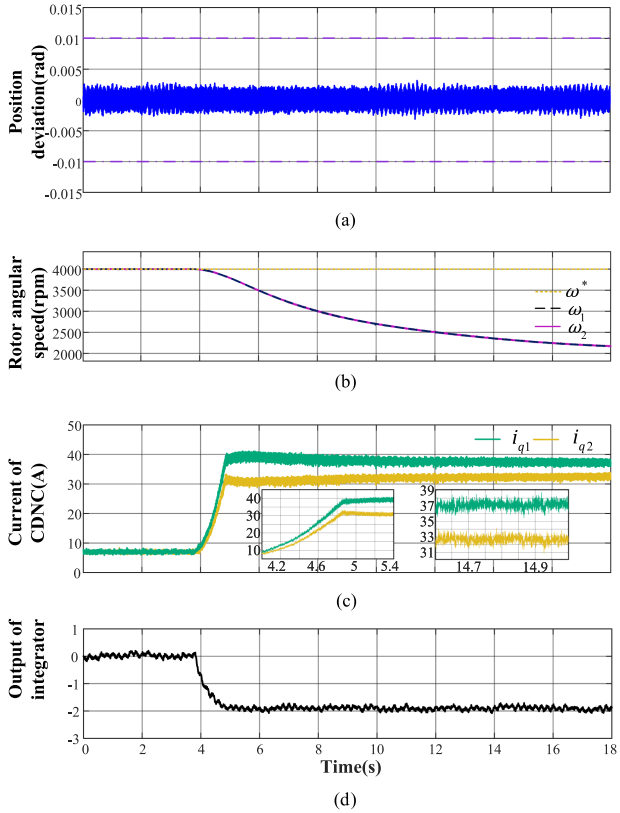


Fig. 17. Control performances of CDNC in situation 3. (a) $\delta$. (b) Two motors' speeds. (c) Two motors' $i_q$. (d) Output of nonlinear coupling controller's integrator.

By switching control mode while running, the TCCC method achieves collision-free operation. But the position deviation is still worse than that of CDNC. The control parameters of TCCC method are extremely difficult to tune in practice. Moreover, As shown in Fig. 16, TCCC method also exhibits poor effectiveness under loading and collision scenarios, resulting in irreversible collision. Hence, we do not report the detailed results of TCCC in situation 3 and 4 here.

Fig. 17 shows the experiment result of CDNC in situation 3. After adding unbalanced load on the two motors, $\delta$ still maintains within an ideal range. The integrator regulates the dc component in the $T_{Ld}^{*}$, which is shown as Fig. 17(d). The CM loop is involved

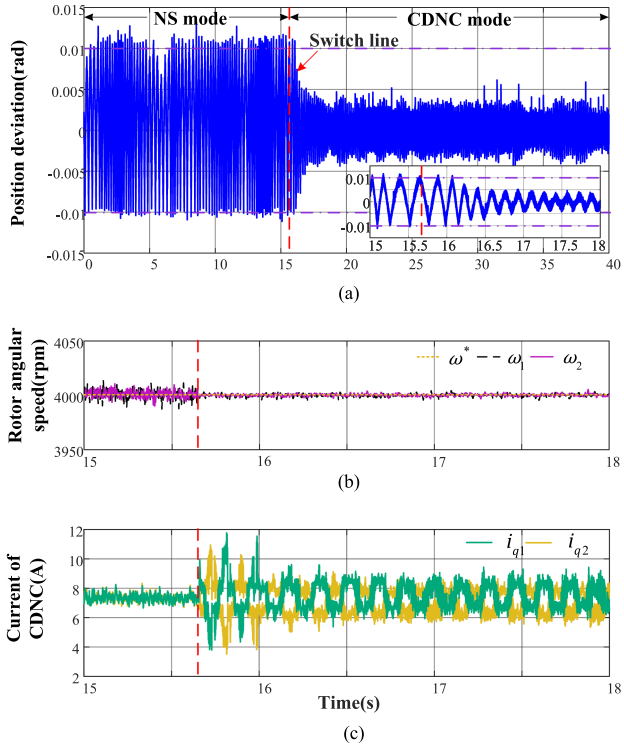


Fig. 18. Control performances of CDNC in situation 4 (4000 r/min). (a) $\delta$. (b) Two motors' speeds. (c) Two motors' $i_q$ .

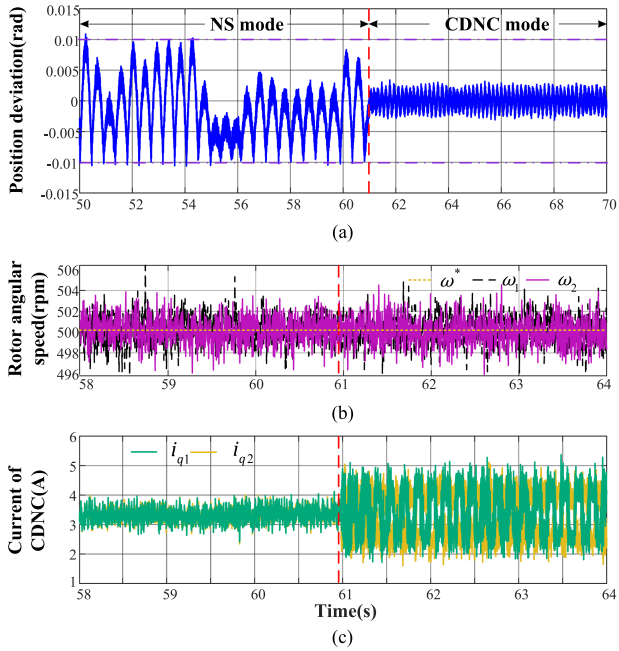


Fig. 19. Control performances of CDNC in situation 4 (500 r/min). (a) $\delta$. (b) Two motors' speeds. (c) Two motors' $i_q$.

at the same time. The nonlinear function proposed in Section III provides an excellent dynamic performance.

To investigate the effect of restitution coefficient, we switch control mode to NS to produce collisions, then switch back to CDNC. Fig. 18 shows the position deviation and corresponding current in situation 4. Under NS mode, CM loop does not participate in collision adjustment. In the early stages after switching mode, variable parameter $k_1$ is large and $r$ in (16) is small. With the joint effect of the two, collision begins to recover. The collision completely ends less than one second after switching to CDNC. As $\delta$ continues to converge, $k_1$ gradually decrease and $r$ approaches toward one, the nonlinear function reaches (20). After a period of time, the oscillation frequency of $\delta$ becomes very high, the current reaches the state shown in Fig. 15(b). This process is consistent with the analysis in Section V.

Collision recovery at low speeds is also tested. As shown in Fig. 19, the frequency and impulse force of collision are significantly reduced compared to those at higher speeds. The collision immediately recovers after switching control mode. The proposed control strategy exhibits better control performance at lower speeds.

## VII. Conclusion

This article proposed a nonlinear CCC strategy based on CM/DM separation to achieve high-accuracy position synchronization under speed control for dual-motor system. The CM/DM-CCC is developed to decouples the objectives of synchronization control and speed tracking. The nonlinear controller is designed to realize fast response, satisfactory steady-state performance, and collision recovery. The stability of system is proved. The method for tuning the control parameters and the analysis of anti-disturbance are presented. Experiments demonstrate that the proposed strategy has better synchronization performance than TCCC under multiple working conditions. Collision recovery is also successfully tested. The proposed control strategy is not limited to the dual-motor structure used in this article. CM/DM separation and nonlinear control can be applied to other synchronization scenarios.

The proposed control strategy has a relatively small computational amount and convenient parameter tuning, making it suitable for industrial applications. Moreover, it can be extended to synchronization of multimotor system.

## References

[1] M. Järvisalo, T. Ahonen, J. Ahola, A. Kosonen, and M. Niemelä, "Soft-sensor-Based flow rate and specific energy estimation of industrial variable-speed-driven twin rotary screw compressor," *IEEE Trans. Ind. Electron.*, vol. 63, no. 5, pp. 3282–3289, May 2016.

[2] Q. Wu, L. Yu, Y. Wang, and W. Zhang, "LESO-based position synchronization control for networked multi-axis servo systems with time-varying delay," *IEEE/CAA J. Automatica Sinica*, vol. 7, no. 4, pp. 1116–1123, Jul. 2020.

[3] S. J. Meitner, L. R. Baylor, and W. D. McGinnis, "R&D extruder developments for the wendelstein 7-X continuous pellet fueling system," *IEEE Trans. Plasma Sci.*, vol. 50, no. 6, pp. 1957–1961, Jun. 2022.

[4] Z. Ye, Z. Zeng, C. Lei, Y. Zhao, and Y. Pang, "Analysis of operating performance parameters of the internal twin screw pump," *Iranian J. Sci. Technol. Trans. Mech. Eng.*, vol. 48, no. 3, pp. 957–970, Sep. 2024.

[5] W. Qin, S. Li, H. Bai, and S. Jia, "Structural design and heat transfer analysis of twin-screw extrusion 3D printer," *Int. J. Adv. Manuf. Technol.*, vol. 130, no. 11, pp. 5601–5618, Feb. 2024.

[6] R. D. Valentine, J. G. Trasky, and D. R. Rippin, "Load sharing of dual motor grinding mill drives," *IEEE Trans. Ind. Appl.*, vol. IA-13, no. 2, pp. 161–168, Mar. 1977.

[7] T.-I. Yeam and D.-C. Lee, "Design of sliding-mode speed controller with active damping control for single-inverter Dual-PMSM drive systems," *IEEE Trans. Power Electron.*, vol. 36, no. 5, pp. 5794–5801, May 2021.
[8] Y. Lee and J.-I. Ha, "Control method of monoinverter dual parallel drive system with interior permanent magnet synchronous machines," *IEEE Trans. Power Electron.*, vol. 31, no. 10, pp. 7077–7086, Oct. 2016.
[9] D. Xiao, X. Li, and K. He, "Power balance of starting process for pipe belt conveyor based on master-slave control," *IEEE Access*, vol. 6, pp. 16924–16931, 2018.
[10] P. Shi, W. Sun, X. Yang, I. J. Rudas, and H. Gao, "Master-slave synchronous control of dual-drive gantry stage with cogging force compensation," *IEEE Trans. Syst., Man, Cybern. Syst.*, vol. 53, no. 1, pp. 216–225, Jan. 2023.
[11] S. Lin, Y. Cai, B. Yang, and W. Zhang, "Electrical line-shafting control for motor speed synchronization using sliding mode controller and disturbance observer," *IET Control Theory Appl.*, vol. 11, no. 2, pp. 205–212, Jan. 2017.
[12] Y. Koren, "Cross-coupled biaxial computer control for manufacturing systems," *J. Dyn. Syst., Meas., Control*, vol. 102, no. 4, pp. 265–272, Dec. 1980.
[13] F. Niu, K. Sun, S. Huang, Y. Hu, D. Liang, and Y. Fang, "A review on multimotor synchronous control methods," *IEEE Trans. Transp. Electrific.*, vol. 9, no. 1, pp. 22–33, Mar. 2023.
[14] Y. Gao, F. Bu, Z. Yang, R. Shi, and W. Huang, "Improved speed synchronization control algorithm based on cross coupling for dual servo motors control," in *Proc. Int. Conf. Elect. Machines Syst.*, Oct. 2018, pp. 2777–2780.
[15] C. Zhu, Q. Tu, C. Jiang, M. Pan, and H. Huang, "A cross coupling control strategy for dual-motor speed synchronous system based on second order global fast terminal sliding mode control," *IEEE Access*, vol. 8, pp. 217967–217976, 2020.
[16] S.-M. Wang, R.-J. Wang, and S. Tsooj, "A new synchronous error control method for CNC machine tools with dual-driving systems," *Int. J. Precis. Eng. Manuf.*, vol. 14, no. 8, pp. 1415–1419, Aug. 2013.
[17] Y. Wu, Y. Cheng, and Y. Wang, "Research on a multi-motor coordinated control strategy based on fuzzy ring network control," *IEEE Access*, vol. 8, pp. 39375–39388, 2020.
[18] Z. Wang, C. Hu, Y. Zhu, S. He, M. Zhang, and H. Mu, "Newton-ILC contouring error estimation and coordinated motion control for precision multiaxis systems with comparative experiments," *IEEE Trans. Ind. Electron.*, vol. 65, no. 2, pp. 1470–1480, Feb. 2018.
[19] S. Zou, W. Zhao, C. Wang, W. Liang, and F. Chen, "Tracking and synchronization control strategy of vehicle dual-motor steer-by-wire system via active disturbance rejection control," *IEEE/ASME Trans. Mechatron.*, vol. 28, no. 1, pp. 92–103, Feb. 2023.
[20] Y. Luo, D. Liang, L. Zhang, S. Cai, and K. Zhou, "Speed synchronized control of dual motors system using fuzzy logic," in *Proc. Int. Power Electron. Motion Control Conf.*, Nov. 2020, pp. 2525–2529.
[21] H. Dou, H. Lu, S. Wang, Q. Liu, D. Wang, and L. Meng, "Research on synchronous control of gantry-type dual-driving feed system based on fuzzy single neuron PID cross-coupled controller," in *Proc. Adv. Inf. Technol., Electron. Automat. Control Conf.*, 2021, pp. 1107–1112.
[22] F. Niu et al., "Cooperative predictive position control of dual-motor system," *IEEE Trans. Emerg. Sel. Topics Power Electron.*, vol. 10, no. 6, pp. 7560–7568, Dec. 2022.
[23] C. Yang, F. Meng, H. Zhang, J. Zhao, H. Wang, and L. Zhou, "Optimal coordinated control for speed tracking and torque synchronization of rigidly connected dual-motor systems," *IEEE/ASME Trans. Mechatron.*, vol. 28, no. 5, pp. 2609–2620, Oct. 2023.
[24] T. Zeng, X. Ren, and Y. Zhang, "Fixed-time sliding mode control and high-gain nonlinearity compensation for dual-motor driving system," *IEEE Trans. Ind. Inform.*, vol. 16, no. 6, pp. 4090–4098, Jun. 2020.
[25] Z. Hao, X. Li, X. Cao, Y. Gan, Q. Yu, and Q. Zhang, "A cross-coupled control strategy of phase difference for electric vibration damping actuator," *IEEE Access*, vol. 8, pp. 213887–213898, 2020.
[26] B. Wang, M. Iwasaki, and J. Yu, "Command filtered adaptive backstepping control for dual-motor servo systems with torque disturbance and uncertainties," *IEEE Trans. Ind. Electron.*, vol. 69, no. 2, pp. 1773–1781, Feb. 2022.
[27] M. L. Corradini, G. Ippoliti, S. Longhi, and G. Orlando, "A quasi-sliding mode approach for robust control and speed estimation of PM synchronous motors," *IEEE Trans. Ind. Electron.*, vol. 59, no. 2, pp. 1096–1104, Feb. 2012.
[28] D. W. Jordan and P. Smith, *Nonlinear Ordinary Differential Equations: An Introduction for Scientists and Engineers*, 4th ed. New York, NY, USA: Oxford Univ. Press, 2007, ch. 7, pp. 225–230.
[29] X. Sun, Y. Tang, X. Xiao, and Y. Xie, "Predictive trajectory control strategy for permanent magnet synchronous motor drives based on deadbeat predictive flux linkage control method," *IEEE Trans. Power Electron.*, vol. 38, no. 2, pp. 2327–2338, Feb. 2023.

**Shuai Li** (Student Member, IEEE) received the B.S. degree in electrical engineering from the China University of Mining and Technology, Xuzhou, China, in 2022. He is currently working toward the M.Eng. degree in electrical engineering with the Chongqing University, Chongqing, China.

His research interests include multimotor control and low carrier ratio.

**Xuewei Xiang** (Member, IEEE) received the B.S. degree from Chongqing University, Chongqing, China, in 2015 and the Ph.D. degree from Tsinghua University, Beijing, China, in 2021, both in electrical engineering.

From 2019 to 2020, he was a visiting Ph.D. student with the Institute for Energy Systems, School of Engineering, University of Edinburgh, Edinburgh, U.K. He is currently an Associate Professor with the School of Electrical Engineering, Chongqing University. His research interests include the design and control of electric machines.

**Hui Li** (Member, IEEE) received the Ph.D. degree in electrical engineering from Chongqing University, Chongqing, China, in 2004.

From 2005 to 2007, he was a Postdoctoral Research Fellow with the Institute of Energy Technology, Aalborg University, Aalborg, Denmark. Since 2008, he has been a Professor with the Department of Electrical Machinery and Electrical Apparatus, School of Electrical Engineering, Chongqing University, where he has also been the Vice Director of the State Key Laboratory of Equipment and System Safety of Power Transmission and Distribution and New Technology. His current research interests include power electronic devices, wind power generation, MMC-HVDC, and grid integration.

**Yunyan Wu** received the B.S. degree in electrical engineering from the China University of Mining and Technology, Xuzhou, China, in 2021. She is currently working toward the M.Eng. degree in electrical engineering with the Chongqing University, Chongqing, China.

Her research interests include deadbeat control of PMSMs.